Report
R-16-07
May 2018

Precipitation of late blooming phases in iron-based alloys

Theoretical modelling

Pavel Korzhavyi
Oleg Gorbatov
Malin Selleby

SVENSK KÄRNBRÄNSLEHANTERING AB

SWEDISH NUCLEAR FUEL
AND WASTE MANAGEMENT CO

Box 3091, SE-169 03 Solna
Phone +46 8 459 84 00
skb.se

SVENSK KÄRNBRÄNSLEHANTERING

ISSN 1402-3091
SKB R-16-07
ID 1557099
May 2018

Precipitation of late blooming phases in iron-based alloys

Theoretical modelling

Pavel Korzhavyi, Oleg Gorbatov, Malin Selleby
Department of Materials Science and Engineering,
KTH Royal Institute of Technology

Abstract

Precipitation of Cu particles in α-Fe is a well-known problem in reactor pressure vessel (RPV) steels. At later stages, precipitation of more complex intermetallic phases has been reported, and those have been termed “late blooming” phases (LBP). Recently, it was suggested that similar ageing processes may also be of importance for the cast iron insert of the canister for long-term disposal of nuclear waste.

These alloy problems can be addressed using the Calphad approach which is based on modelling thermodynamic descriptions using experimental data. In order to make more reliable predictions at low temperatures, the Calphad approach can be combined with the *ab initio* approach which is based on quantum mechanics and density functional theory. A combination of these two approaches is used in this study to analyze the phase composition of the cast iron insert material intended for use in nuclear waste disposal applications. The analysis shows that precipitation of several phases such as the G-phase (rich in Ni, Mn, and Si), M_2P and M_3P phosphides (M = Cr, Fe, Ni), and Mn-containing sulfide is thermodynamically possible. The equilibrium volume fraction of G-phase precipitates below 200 °C is found to be limited by the amount of Mn and Ni in the studied material and calculated to be about 0.5 %.

Contents

1 Introduction

Irradiation of metallic alloys may cause precipitation and dissolution of alloy phases thus altering the mechanical properties. Precipitation of Cu particles from the α-Fe based solid solution is a well-known problem in reactor pressure vessel (RPV) steels. Precipitation of more complex intermetallic phases in RPV and similar reactor steels has been predicted to occur at later stages; such precipitates have been termed "late blooming" phases (LBP) (Odette and Nanstad 2009). Experimentally, nanometer-sized clusters (enriched in Ni, Si and Mn) were observed to form preferentially at lattice defects such as dislocations and grain boundaries in reactor steels (Miller and Russell 2007, Sencer et al. 2009). The exact atomic structure and composition of these precipitates are uncertain.

Different opinions have been expressed concerning thermodynamic stability of LBPs and their potential influence on the mechanical properties of RPV steels. Atomistic modelling studies, based on defect interactions obtained from *ab initio* calculations, have shown that irradiation-induced clustering of point defects in Fe-Cu-Ni-Mn solid solutions produces very stable copper-rich precipitates (CRP), whereas Ni-Mn-rich precipitates are either unstable or just barely stable (Bonny et al. 2013). However, Ni and Mn solutes are found to form stable segregations at the interface between the Cu-rich precipitates and the Fe matrix, thus promoting Cu precipitation (Gorbatov et al. 2015). More stable Ni-Mn-Si-rich (NMS) clusters are reported to form in the atomistic modelling studies of Fe-based solutions additionally containing Si and P impurities (Ngayam-Happy et al. 2013). These clusters may be precursors of thermodynamically stable Ni-Mn-Si phases whose precipitation from Fe-based solid solution is predicted by Xiong et al. (2014) using the CALculation of PHAse Diagrams (Calphad) method (Saunders and Miodownik 1998, Lukas et al. 2007). Sufficient experimental evidence exists for the formation of Ni-Mn-Si-enriched clusters (often identified as the G-phase) in high-fluence irradiated RPV steels (Miller and Russell 2007, Miller et al. 2009, Was et al. 2014, Wells et al. 2014, Styman et al. 2015, Gurovich et al. 2015, Sprouster et al. 2016, Lindgren et al. 2017). The effect of NMS clustering on the mechanical properties of RPV is well established, (Odette and Nanstad 2009, Miller et al. 2009, Lindgren et al. 2017). Post-irradiation annealing at temperatures above 450 °C causes dissolution of NMS clusters, which occurs more rapidly at higher temperatures and is accompanied by a recovery of the mechanical properties (Styman et al. 2015).

Precipitation during annealing or tempering of Cu-bearing high-alloy steels has some similarities with irradiation-induced clustering in RPV steels. In these steels, which typically have significantly higher content of Cu, Ni, Mn, Al, Si and other alloying elements than RPV steels, the ageing processes occur rapidly to produce nanometer-sized Cu-rich clusters that are co-located with Ni-rich precipitates of Ni-Mn-Al (Kolli and Seidman 2008) and Ni-Ti-Al-Si (Stiller et al. 2008) intermetallic phases or with M_2C carbide nanoparticles {M = Cr, Mo, Co, Ti} (Mulholland and Seidman 2011). Formation of the G-phase, with composition similar to $Ni_{16}Ti_6Si_7$, has been reported to occur at late stages of ageing (Stiller et al. 2008). The ageing processes in these precipitation-strengthened steels are characterized by a high number density, small size, long-term evolution of phase composition, and slow coarsening rate of the precipitates (Kolli and Seidman 2008, Stiller et al. 2008, Mulholland and Seidman 2011).

Recently, it was suggested that similar processes of solute clustering and precipitation may be important for the iron insert of the canister for long-term disposal of nuclear waste (SSM 2011). In the KBS-3 repository the canister shall contain the spent nuclear fuel and prevent the release of radioactive substances into the surroundings. The main roles of the nodular cast iron insert (together with its lid made of structural steel) are to provide mechanical rigidity to the canister (while keeping high ductility), to shield radiation, and to prevent criticality.

SKB have requirements for certain material properties such as strength and ductility (SKB 2010). To avoid gamma irradiation induced hardening and embrittlement in the cast iron the copper content in nodular cast iron shall be < 0.05 % (see Table 3-1). Also, to ensure that that criticality will not occur, in nodular cast iron the iron content shall be > 90 %, the carbon content < 6 %, and silicon content < 4 %. Thus, the composition of the canister insert material is different from those of RPV steels and precipitation-strengthened steels, so the question of precipitation requires a separate investigation to take into account the composition of the material and irradiation conditions.

The main goal of the present study is to estimate the possibility of irradiation-stimulated precipitation of LBPs in the nodular cast iron in the range of temperatures 0–125 °C corresponding to the conditions of nuclear waste disposal (SKB 2010). The problem of LBP precipitation is studied here using two complementary approaches, the one based on the analysis of *ab initio* calculated data on point defect interactions in bcc Fe-based solid solutions, and the Calphad approach based on the thermodynamic data available for iron and steel. Another goal is to analyze whether the predictions of the two modelling approaches are consistent with each other, as well as to identify the scientific techniques that could be used to get more accurate estimates.

2 Point defect interactions in bcc Fe

Knowledge of interactions between solute atoms (as well as with other point defects such as vacancies and self-intersititals) is important for analysing the impurity diffusion, as well as the structure and kinetics of solute-defect clusters and precipitate phases that may form during the decomposition of a supersaturated solid solution on its way to the equilibrium or steady state. For example, in the case of the bcc structure, strong and attractive solute–vacancy interactions on the first and second nearest-neighbour shells lead to the formation of a bound solute–vacancy complex that does not dissociate in the course of nearest-neighbour atom–vacancy exchanges, thereby promoting an accelerated solute (or impurity) diffusion in the alloys.

Several *ab initio* based studies of point defect interactions and their effects on the kinetics and thermodynamics of precipitation phenomena in bcc Fe have been performed (Domain and Becquart 2001, Domain 2006, Soisson and Fu 2007, Ohnuma et al. 2009, Olsson et al. 2010, Gorbatov et al. 2011, 2013, 2015, 2016, Messina et al. 2014, 2016). Most of the published data are consistent with each other and with the data presented and discussed in Section 2.2 to 2.3.

2.1 Necessary definitions

Effective interactions of solute atoms with each other indicate the tendency of the solute atoms to arrange themselves in the crystal lattice of the solvent (in this case, the bcc Fe matrix). In the dilute alloy case, the pair interaction energy of impurities A and B, $V_{AB}(R_i)$, may be defined as the total energy of a system where these impurities are separated by the distance R_i of the i-th coordination shell radius (discrete variable), minus the energy of the same system with the two impurities infinitely separated.

By the definition given above, a negative sign of interaction energy $V_{AB}(R_i)$ means that the total energy is lowered when two dissociated solutes form a pair in which they are separated by the distance R_i from each other ("attractive" interaction). On the contrary, a positive sign of the interaction energy corresponds to "repulsion" between the two solutes. Usually, solute–solute interaction energy exhibits a damped oscillatory behaviour as a function of distance (Olsson et al. 2010, Messina et al. 2014). The magnitude of these oscillations becomes small beyond the second coordination shell, so that a few nearest-neighbour interactions are usually sufficient for a qualitative analysis of the ordered arrangements of solute atoms at low temperatures. The composition and structure of these arrangements may be indicative of the composition and structure of the phases that have the tendency to precipitate out of the solid solution.

2.2 Calculation details

Pair interaction energies of point defects (substitutional impurities and vacancies) in bcc iron were obtained by means of *ab initio* calculations employing a supercell approach. Every defect pair was considered in a 128-site supercell obtained by the $4 \times 4 \times 4$ repetition of a body-centered cubic unit cell and containing two defects separated from each other by the distance of the i-th coordination shell radius (i = 1, 2, 3), see Figure 2-1. The interaction energy at the i-th coordination shell (c.s.) was computed as the difference between the total energy of the corresponding supercell and that of a similar supercell containing the same defect pair in a dissociated configuration (separated by the largest possible distance within the given supercell). The convergence with respect to the supercell size was verified, in some critical cases, against similar calculations using 432-site ($6 \times 6 \times 6$) supercells. The total energies were computed in the generalized gradient approximation (GGA) (Perdew et al. 1996) which correctly predicts the ferromagnetic bcc structure to be the ground state of iron and closely reproduces its equilibrium atomic volume. The electronic structure calculations employed the locally self-consistent Green's function (LSGF) method with a linear scaling of computational time with the number of atoms N, a so-called order-N method (Abrikosov et al. 1996, 1997). Each atom of the supercell, together with three coordination shells of atoms around it, was considered self-consistently as a local interaction zone (LIZ) embedded in the effective medium of the LSGF method.

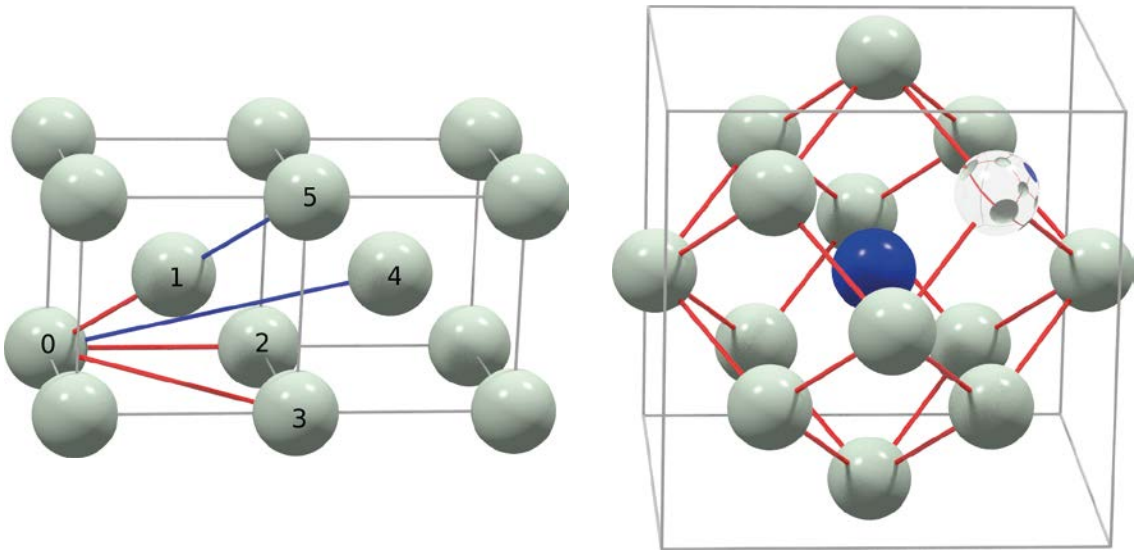

Figure 2-1. *a) First five coordination shell radii in the bcc lattice (the separation distances considered in this study are indicated by red color). b) First two coordination shells of atoms (gray balls) around an impurity (blue ball) bound to a vacancy (glass ball) in the bcc lattice. Red sticks indicate possible non-dissociative vacancy jumps around the impurity.*

This LIZ size is necessary for studying point defect interactions at the distance of up to the third coordination shell radius. Although the convergence of the calculated interactions with respect to the LIZ size cannot be proved in general, it has been tested to be sufficient in some important cases studied (Gorbatov et al. 2011, Gorbatov et al. 2016). Taking the results of these tests into account, the technical numerical accuracy of the interaction energies presented in this report can be estimated as ± 0.03 eV. This does not include the errors related to other approximation used such as the neglect of lattice relaxation around point defects (Gorbatov et al. 2016), GGA, and the neglect of finite-temperature effects (we note that the magnitude of thermal fluctuations at room temperature is also of the order of 0.03 eV).

2.3 Interaction energies and clustering tendency

Interatomic distances corresponding to the first five coordination shell radii in the bcc lattice of iron are indicated by lines in Figure 2-1(a). Point defect interactions calculated in this work for the first three coordination shells in bcc Fe are listed in Tables 2-1 and 2-2, in comparison with the results of previous calculations. The solute–solute interactions presented in Table 2-1 have been calculated in the dilute alloy limit and can be used as indicators of stability of dilute Fe-X solid solutions. For instance, the repulsive interactions calculated for Cr-Cr solute pairs indicate that dilute Fe-Cr solid solutions are stable against solute clustering and exhibit an ordering tendency, in agreement with *ab initio* studies of Fe-Cr alloys (Olsson et al. 2003, 2006, Ruban et al. 2008). A weaker ordering tendency has been reported for Mn by Gorbatov et al. (2013, 2016) whereas calculations by Olsson et al. (2010) suggest a clustering tendency of Mn solutes in dilute Fe-Mn solid solutions. The observed discrepancy is probably related to the fact that different spin moment configurations of Mn solutes and solute pairs are very sensitive to the details of calculations. In our LSGF and VASP-PAW calculations (Gorbatov et al. 2016) Mn impurities are found to prefer to couple antiferromagnetically to the iron matrix, irrespective of the atomic configuration, whereas Olsson et al. (2010) report a ferromagnetic coupling for isolated Mn impurities to the Fe matrix.

All calculations predict very weak interactions for Ni–Ni solute pairs in iron. This result indicates that dilute Fe-Ni solid solutions are stable as random solid solutions without any significant ordering or clustering tendency. In contrast, strong attractive interactions that are obtained for Cu–Cu solute pairs in Fe indicate a strong clustering tendency of the solutes which is consistent with the formation of copper-rich precipitates in steels under irradiation or during annealing.

Solutes from the 3*sp* series (namely, Si, P and S) exhibit a strong repulsion on the first coordination shell and a weaker attractive interaction on some of the more distant shells. Such behaviour of interaction energy indicates that these solutes tend to form ordered compounds with the solvent. This conclusion agrees with the strong ordering effects in the binary solid solutions, e.g. B2 (CsCl-type) ordering in bcc Fe-Si, as well with the existence of stable binary compounds, such as Fe_2Si, FeSi, Fe_3P, Fe_2P, FeP, FeS, and FeS_2, as well as multicomponent Fe(Si, P), $(Fe, Cr)_2P$, and $(Fe, Mn, Cr)_3P$ phases.

Table 2-1. Interaction energy (eV) between two solutes X in ferromagnetic bcc Fe, calculated as a function of X–X separation distance for the first three coordination shells (c.s.). The strongest interactions for each element are indicated in bold.

c.s.	Cr	Mn	Ni	Cu	Si	P	S	Reference
1	**+0.24**	+0.10	**+0.03**	**–0.17**	**+0.34**	**+0.57**	**+0.45**	Gorbatov et al. 2013.
2	+0.11	**+0.11**	–0.01	–0.08	+0.11	+0.11	–0.10	
3	+0.03	+0.05	+0.03	+0.01	–0.03	–0.01	+0.04	
1	**+0.24**	**–0.08**	**–0.02**	**–0.25**				Olsson et al. 2010.
2	+0.12	–0.04	+0.00	–0.06				
3	+0.04	+0.00	+0.02	–0.02				

Table 2-2. Vacancy-solute interaction energy (eV) for selected solute atoms in ferromagnetic bcc Fe, calculated as a function of Va–X separation distance for the first three coordination shells (c.s.). The strongest interactions for each element are indicated in bold.

c.s.	Cr	Mn	Ni	Cu	Si	P	S	Reference
1	**–0.05**	**–0.17**	–0.14	**–0.26**	**–0.24**	**–0.32**	**–0.55**	Gorbatov et al. 2011 and present work.
2	–0.03	–0.10	**–0.20**	–0.21	–0.12	–0.27	–0.44	
3	+0.01	+0.01	+0.01	+0.01	+0.03	+0.05	+0.07	
1	**–0.06**	**–0.21**	–0.12	**–0.27**				Olsson et al. 2010.
2	–0.01	–0.14	**–0.20**	–0.16				
3	–0.00	–0.06	–0.03	–0.03				
†	**–0.05**	**–0.16**	**–0.19**	**–0.24**	**–0.29**	**–0.36**	**–0.53**	Ohnuma et al. 2009.

† First or second (Ni) coordination shell distance to the vacancy.

Table 2-3. Selected interactions of X-Y solute pairs in the bcc crystal lattice of Fe for the first three coordination shells (c.s.). The strongest interactions for each element are indicated in bold.

	c.s.	Cr	Mn	Ni	Cu
Si	1	**+0.09**	–0.05	**–0.08**	**–0.09**
	2	+0.07	**+0.09**	+0.06	+0.00
	3	+0.01	+0.01	+0.02	+0.00
P	1	+0.02	–0.10	**–0.05**	**–0.06**
	2	**+0.08**	**+0.20**	+0.03	–0.05
	3	+0.01	+0.02	+0.03	+0.01
S	1	–0.04	–0.12	**–0.07**	–0.09
	2	**+0.10**	**+0.15**	–0.04	**–0.12**
	3	+0.02	+0.03	+0.03	+0.01

Similar to Cu impurities, the 3*sp* impurities have attractive interactions with vacancies (see Table 2-2). It is noteworthy that the vacancy–solute interactions are attractive (and of similar strength) at both the first and the second coordination shell distance. Because of this, the vacancy can make nearest-neighbour exchanges not only with the impurity to which it is bound, but also with the host atoms surrounding the impurity, without breaking the vacancy-impurity pair, see Figure 2-1(b). Thus, strong attractive interactions on the first and second coordination shells make vacancy–P and vacancy–S pairs stable and mobile defect complexes, which explains why P and S impurities are fast diffusers in bcc iron (Bakker et al. 1990). It should be added that recent careful analyses of diffusion mechanisms show that attractiveness of the first two vacancy–impurity interactions is not a necessary condition for fast diffusion of the impurity in the bcc host lattice (Messina 2014, 2016).

As comparison of the data between Tables 2-1 and 2-2 shows, the attractive interactions of Si, P and S impurities with vacancies in Fe are of the same magnitude as the repulsive solute–solute interactions. Therefore, one can expect vacancies not only to accelerate the diffusion of these impurities in iron, but also to become part of the structure of concentrated defect arrangements and precipitate phases such as silicides, phosphides, or sulphides.

The structure of two concentrated defect arrangements of Si in bcc Fe, with composition close to Fe_2Si, have been reported: one approximately described as a bcc-based (Pearson symbol *cI2*, space group #299, a = 2.81 Å,) random solid solution $Fe_{0.67}Si_{0.33}$ (Frolov et al. 1972) and the other that shows partial B2-type order (*cP2*, #221, a = 2.81 Å), with one primitive cubic sublattice fully occupied by Fe and the other sublattice jointly occupied by Fe and Si, to give the total composition $Fe_{1.34}Si_{0.66}$ (Khalaff and Schubert 1974). The vacancy content of these two concentrated arrangements is unknown, but the structure of a fully ordered, hexagonal Fe_2Si phase (*hP6*, #164, a = 4.053, c = 5.0855 Å) has been reported by Kudielka (1977). The hexagonal Fe_2Si phase can still be related to the body-centred cubic matrix phase *via* the Heusler alloy structure, as exemplified in Figures 2-2 (a) and (b). The "cubic" representation of the hexagonal Fe_2Si phase shown in Figure 2-2 (b) has a vacancy content of 25 %, which corresponds to the low weight density of Fe_2Si (6.42 g/cm^3) as compared to the density expected of concentrated substitutional $Fe_{0.67}Si_{0.33}$ bcc arrangements without vacancies (6.75–6.99 g/cm^3).

The structures of orthorhombic Fe_4P phase (*oP5*, #47, a = 3.59 b = 4.01, c = 4.32 Å) reported by Hornbogen (1961) and tetragonal Fe_3P phase (*tI32*, #82, a = 9.107 c = 4.460 Å) reported by Rundqvist (1962) appear to be very different from the bcc crystal structure of the iron matrix. However, the calculated P–P and vacancy–P interactions facilitate clustering of the point defects in the bcc Fe matrix to produce solute-enriched point defect arrangements that may serve as the precursors of the stable phosphide phases.

A number of phases whose structures can be related to the bcc structure of the Fe matrix have been reported experimentally. Thus, the crystal structure of α-MnS reported by Furuseth and Kjekshus (1965) is NaCl-type (*cF8*, #225, a = 5.2226 Å). It has a low weight density of 4.06 g/cm^3 and can be interpreted as a bcc-like ordered arrangement of Mn and S solutes with 50 % vacancy content, as shown in Figure 2-2 (c). The structure of a ternary Heusler alloy phase Fe_2MnSi (*cF16*, #225, a = 5.671 Å) has been reported by Buschow et al. (1983). A number of compositions, some of them Fe-containing, with the structure of G-phase $Ni_{16}Mn_6Si_7$ (*cF116*, #225, a = 11.09 Å) have been reported by Kolenda et al. (1991). Although the structure of the G-phase in Figure 2-2 (d) appears to be quite distorted, one can still resolve the rows of atoms typical of the Heusler alloy phase shown in Figure 2-2 (a). By straightening the atomic rows, one can establish the relationship between these two phases. Thus, the unit cell of the G-phase $A_{64}B_{24}C_{28}$ is a $2 \times 2 \times 2$ multiple of the Heusler alloy unit cell $A_8B_4C_4$, with 8 B and 4 C lattice sites being vacant. Large atomic displacements in the G-phase structure, relative to the Heusler alloy structure, totally obscure the vacancies.

The solute–solute interactions reported in Tables 2-1 and 2-2 are of X–X type, which correspond to effective pair interactions in binary bcc Fe–X solid solutions. To derive the structures of possible ternary precipitate phases, one also needs interactions of X-Y type, i.e. between the different solutes X and Y. Some of the calculated interaction energies for X-Y solute pairs in bcc Fe are listed in Table 2-3. The interactions of 3*sp* solute elements Si, P, and S with Cr solutes in bcc Fe are found to be mostly repulsive, whereas their interactions with Mn are attractive for the first and repulsive for the second coordination shell. The interactions of the 3*sp* solutes with Ni and Cu are mostly attractive. Attractive nearest-neighbour interactions of Cu impurities with Ni and Mn solutes (–0.09 and –0.05 eV, respectively) in Fe have been reported by Gorbatov et al. (2015) and their influence on the Cu precipitation has been studied.

Ab initio calculations of point defect interactions in multicomponent Fe-based alloys are now being performed by several research groups, with the aim to use these interactions in Monte Carlo modelling studies of the structure, thermodynamics, and kinetics of phase precipitation in iron (Bonny 2013, Ngayam-Happy et al. 2013, Gorbatov et al. 2015). An alternative way of exploring the possibility of LBP precipitation in multicomponent Fe-based alloys is to use Calphad modelling based on thermodynamic databases developed for phases in steel (Xiong et al. 2014). The results of such modelling are reported in the next section.

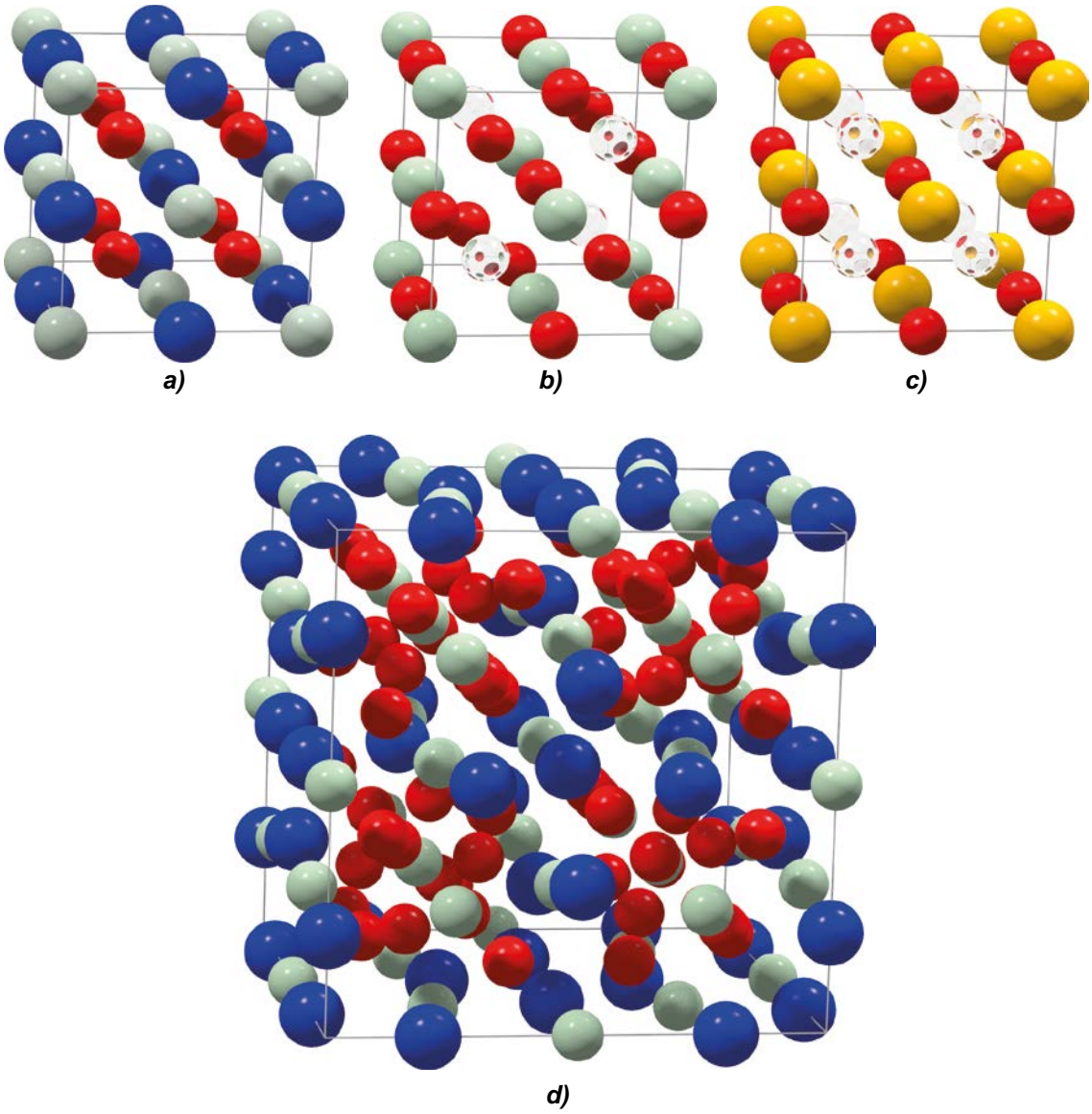

Figure 2-2. *Ball-and-stick models of some potential precipitate structures based on the bcc crystal lattice: a) Heusler alloy Fe_2MnSi (Fe-red, Mn-blue, Si-gray), b) cubic variant of Fe_2Si structure (Fe-red, Si-green), c) rocksalt structure of MnS (Mn-red, S-yellow), and d) G-phase $Ni_{16}Mn_6Si_7$ (Ni-red, Mn-blue, Si-gray). The glass balls show vacant sites in the underlying bcc lattice.*

3 Calphad modelling

3.1 Calculation details

The present Calphad calculations have been performed using the Thermo-Calc software (Andersson et al. 2002). Thermodynamic database TCFE7 (Thermo-Calc Software TCFE7 Steels/Fe-alloys database version 7) has been used.

The alloy composition for the present Calphad calculation has been chosen equal to the mean composition of the nodular cast iron BWR inserts (I53–I57) manufactured in 2007. The BWR insert compositions are listed in Table 5-1 of Canister design report (SKB 2010), and the composition used in the present calculation is given in Table 3-1.

Table 3-1. Material composition (mass-%) used in the present Calphad calculation in comparison with mean values from Table 5-1 in SKB (2010) and the technical specification for test manufacturing of nodular cast iron inserts. A typical value of Cr content in the insert material has been assumed.

	Cu	C	Si	Mn	P	S	Ni	Mg	Cr
Present study	0.04	3.61	2.31	0.15	0.024	0.006	0.39	0.044	0.04
Mean values	0.039	3.62	2.31	0.16	0.024	0.007	0.39	0.044	
Technical specification	≤0.05	3.2–4.0	1.5–2.8	0.05–1.0	≤0.08	≤0.02	≤2.0	0.02–0.08	

3.2 Predicted phase composition

Calphad calculations have been performed to see what phases would have formed under equilibrium conditions at relatively low temperatures in an iron insert with the mean composition (mass-%) i.e. Fe-0.04Cu-3.61C-2.31Si-0.15Mn-0.024P-0.006S-0.39Ni-0.044Mg and an addition of 0.04 mass-% Cr (this amount of chromium is typically present as an impurity in cast iron and carbon steel). Chromium is an extremely potent carbide forming element and the maximum level of Cr which can be accepted in nodular cast iron is 0.05 % (Gagné 2004). Volume fraction of the phases formed in the temperature interval 0–500 °C is shown in Figure 3-1.

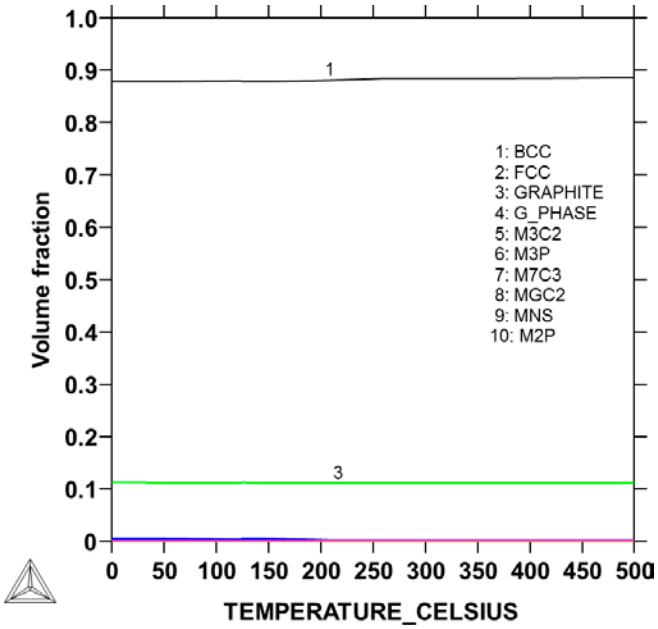

Figure 3-1. *Calculated volume fraction for the primary phases (1: α-Fe matrix, 3: carbon graphite) in equilibrium state of the considered alloy.*

The iron insert of the canister is predicted to have a ferritic matrix with about 11 % graphite and, as shown in Figures 3-2 and 3-3, small fractions of a number of additional phases. We note that the calculated phase fractions correspond to the state of thermodynamic equilibrium. At variance with that, the initial microstructure of the real cast iron, depending on the manufacturing conditions, may involve up to 10 % pearlite where some carbon is bound into a metastable phase Fe_3C (cementite). This will reduce the volume fraction of graphite to values below 10 % and may also affect the volume fractions of minor carbide phases.

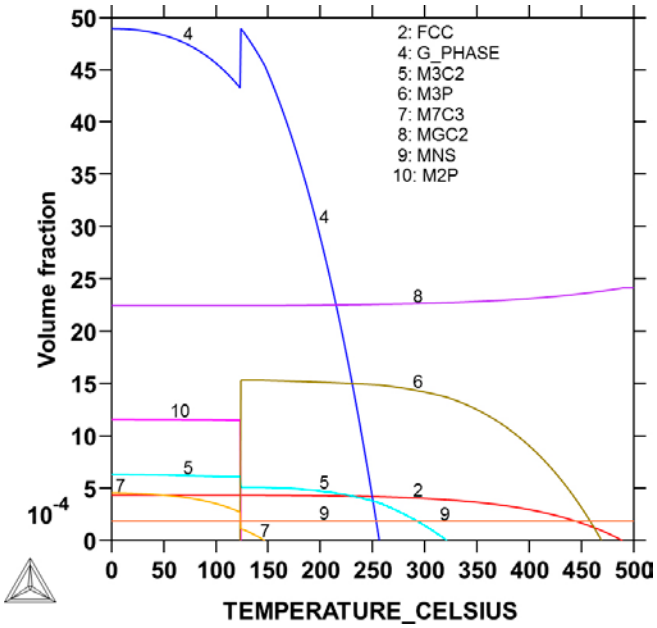

Figure 3-2. *Calculated volume fraction for major precipitate phases (4: G-phase $Ni_{16}Mn_6Si_7$, 8: MgC_2) in equilibrium state of the considered alloy.*

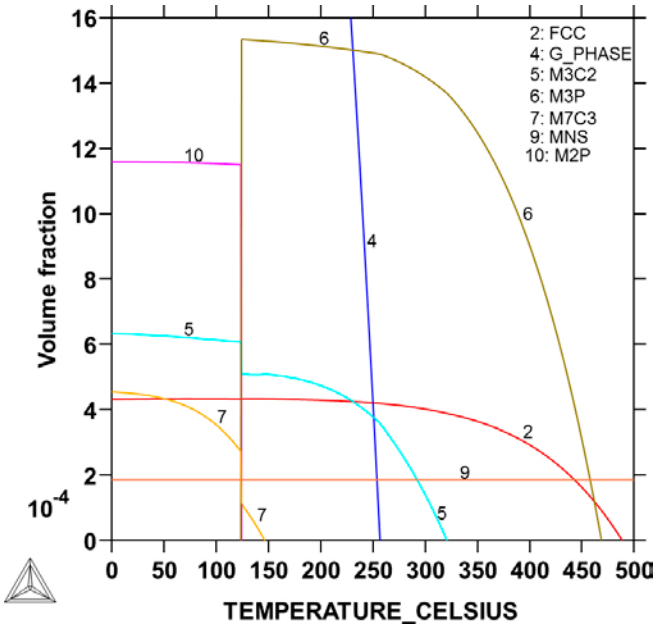

Figure 3-3. *Calculated volume fraction of minor precipitate phases (5: Cr-rich carbide M_3C_2; 7: Ni, Mn-rich carbide M_7C_3; 6: Fe-rich phosphide M_3P, 10:Ni-rich phosphide M_2P; 9: MnS; 2: Cu-rich fcc phase) in equilibrium state of the considered alloy.*

The phases that appear are fcc, G-phase, the carbides M_3C_2, M_7C_3, and MgC_2, the phosphides M_2P, M_3P, and a sulphide named MnS. Their respective models and actual compositions in this case are given in Table 3-2. The content of Cu, Mn, Ni, Mg and Cr (mass fraction) in the different phases is shown in Figures 3-4 through 3-8. The content is only shown in the temperature interval where the phase is stable. In addition to the graphite and carbide phases that are quite expectable, the calculation predicts a relatively large volume fraction (~ 0.5 %) of G-phase to form as a stable phase at temperatures below 250 °C. Phosphide phases are also predicted to become stable at low temperatures (below 450 °C), while the sulfide phase is stable in the whole temperature range considered in this study. Precipitation of fcc copper is also predicted (because of the low solubility of copper in iron at low temperatures), but the corresponding volume fraction is tiny due to the small Cu content in the alloy.

Table 3-2. Calculated equilibrium phase composition of the considered iron alloy at 25 °C.

Phase name	Model	Composition	Comment
BCC	$(Cr, Cu, Fe, Mg, Mn, Ni, P, S, Si)_1(C, Va)_3$	Mainly Fe	Matrix
FCC	$(Cr, Cu, Fe, Mg, Mn, Ni, P, S, Si)_1(C, Va)_1$	Mainly Cu	CRP†
GRAPHITE	C	Only C	
G-phase	$(Fe, Ni)_{16}(Mn)_6(Fe, Ni, Si)_7$	$Ni_{16}Mn_6Si_7$	NMSRP‡
M_3C_2	$(Cr)_3(C)_2$	Cr_3C_2	Carbide
M_7C_3	$(Cr, Fe, Mn, Ni, Si)_7(C)_3$	Close to Mn_7C_3	Carbide
MgC_2	$(Mg)_1(C)_2$	MgC_2	Carbide
M_2P	$(Cr, Fe, Ni)_2(P)_1$	$Fe_{0.26}Ni_{1.73}P$	Phosphide
M_3P	$(Cr, Cu, Fe, Ni)_3(P)_1$	$Cr_{0.18}Fe_{1.86}Ni_{0.96}P$	Phosphide
MnS	$(Cu, Fe, Mg, Mn)_1(S)_1$	MgS	Sulfide

† Cu-rich precipitate.

‡ Ni, Mn, Si-rich precipitate.

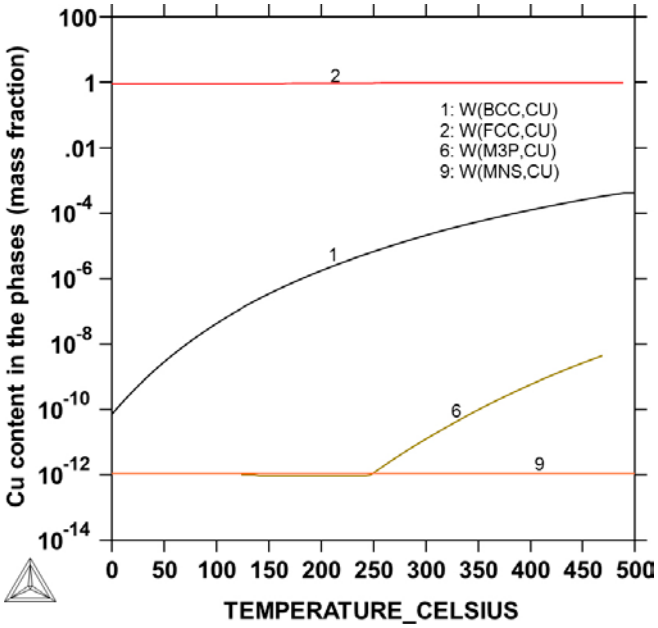

Figure 3-4. *Cu distribution.*

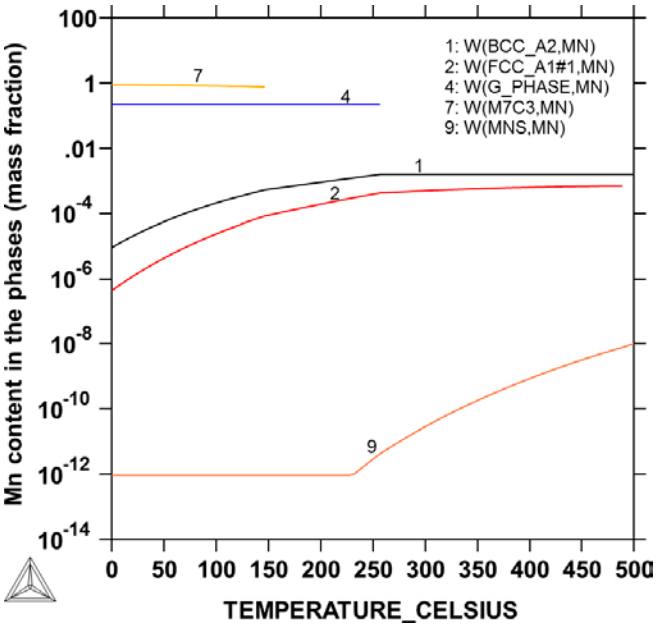

Figure 3-5. *Mn distribution.*

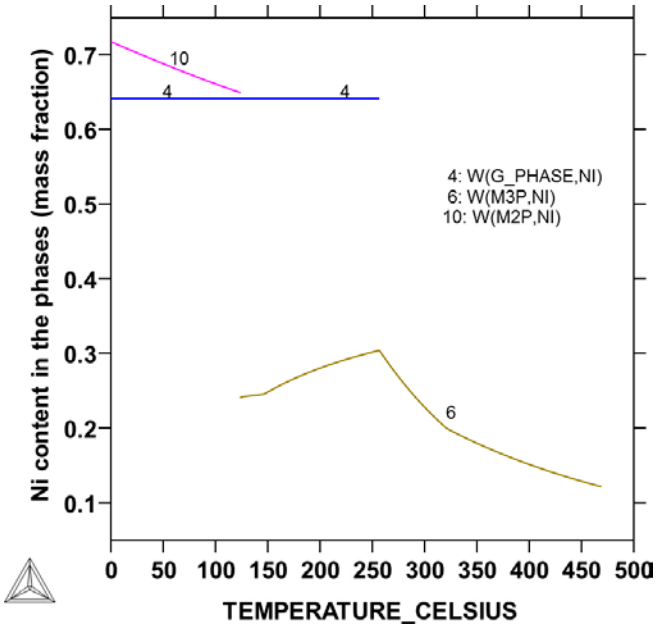

Figure 3-6. *Ni distribution.*

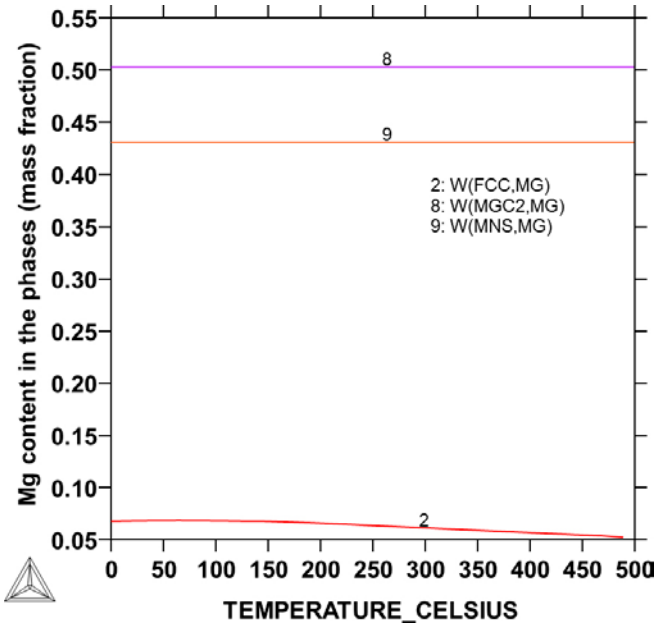

Figure 3-7. *Mg distribution.*

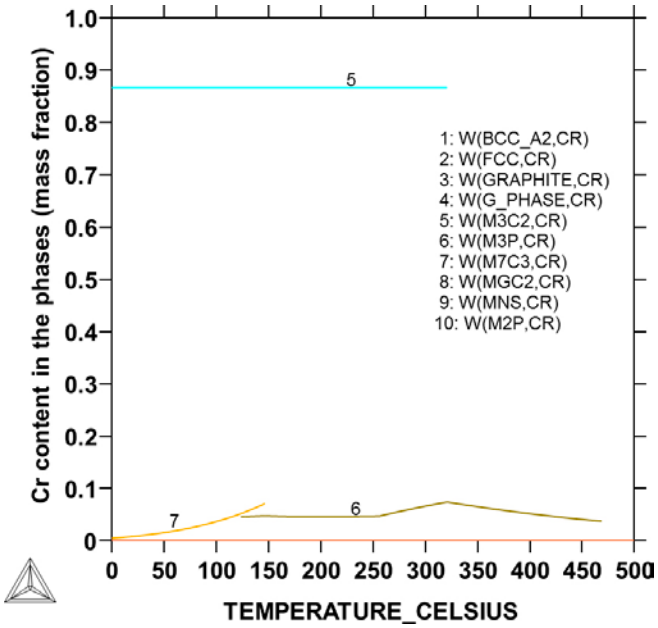

Figure 3-8. *Cr distribution*

4 Discussion

The interaction energies for solute–solute and solute–vacancy defect pairs in ferromagnetic bcc Fe, determined in this work using *ab initio* calculations and supercell geometry, are consistent with the corresponding results of previously published studies by Domain and Becquart (2001), Domain (2006), Ohnuma et al. (2009), Olsson et al. (2010), Bonny et al. (2013), Ngayam-Happy et al. (2013), Gorbatov et al. (2011, 2013, 2015, 2016), and Messina et al. (2014, 2016). So far, these interactions were used for atomistic modelling of Cu precipitation in irradiated binary or multicomponent iron alloys and, most recently, to model LBP precipitation (Bonny et al. 2013, Ngayam-Happy et al. 2013). From these theoretically obtained data one can conclude that the strongest defect interactions, capable of driving solute clustering to form concentrated arrangements of point defects (precursors of LBPs), are those that involve 3*sp* elements (Si, P, S) and vacancies in iron. Mutual interactions of 3*d* solute elements (excluding Cu) in Fe are generally too weak to drive the LPB precipitation (see also Bonny et al. 2013).

Radiation-induced interstitial atoms (dumbbells) are also expected to play an important role in the kinetics of solute clustering. Self-interstitial Fe defects have a higher formation energy, produce larger distortions, and, importantly, have a much higher mobility in the bcc Fe lattice as compared to vacancies. Their interactions with solute atoms have been systematically studied and found to be mostly repulsive (or weakly attractive in some configurations) for 3*d* impurities in Fe, except Cr and Mn which can bind strongly to a dumbbell (Olsson et al. 2010). Similar to the case of P in Fe (Domain and Becquart 2005), Mn and Cr solutes form stable mixed dumbbells (Olsson et al. 2010, Messina et al. 2016) which can migrate with a low energy barrier. Thus, interstitial-mediated diffusion must contribute considerably to the kinetics of solute clustering and precipitation involving Mn, Cr, and P and should therefore be taken into account to predict the nucleation rate and precipitate number density in irradiated materials (Chiapetto et al. 2017).

The structures of concentrated bcc-based arrangements of point defects that can be derived from the strongest interactions in the Fe-based alloys may be related to those of experimentally reported intermetallic phases in the respective binary or ternary Fe-based alloys. Candidate crystal structures include the CsCl-type B2 phase, Heusler and half-Heusler alloys, and some other related structures such as the G-phase. Chemically, these compounds may be silicides, phosphides, or sulphides of Fe, Mn, and Ni (including multicomponent solid-solution phases). The role of vacancies in the precipitation process may be two-fold: as mediators of atomic diffusion in the solid state and as structural elements of the precipitate phases (this also applies to Cu precipitation, see Soisson and Fu 2007). Attractive interactions of vacancies with Si, P, and S impurities can accelerate the impurity diffusion of these elements in irradiated iron alloys at low temperatures.

Because of their relatively high formation energy (Domain 2006), interstitial defects (including less-energetic mixed dumbbells) readily rejoin the crystal lattice at sinks or recombine with vacancies. Less mobile and more stable interstitial clusters involving Cr and Mn solutes have been shown to form in large numbers in irradiated steel (Chiapetto et al. 2017). Upon further growth these clusters are expected to evolve towards lower-energy defect structures such as dislocation loops (Chiapetto et al. 2017, Fikar et al. 2017). In well-developed precipitates, to which the present thermodynamic analysis is applicable, only a tiny fraction of interstitial atoms (Fe or substitutional elements) is expected to be present. Experimental studies show that, at large fluencies, the precipitates in irradiated steels evolve towards the compositions and volume fractions of intermetallic phases expected on the basis of equilibrium thermodynamics (Wells et al. 2014, Xiong et al. 2014, Sprouster et al. 2016, Lindgren et al. 2017).

Empirically-based thermodynamic Calphad modelling, performed in this work for a prototype composition of cast iron insert at temperatures below 500 °C, has revealed that (in addition to graphite and several carbide phases) sulphide phases are stable within the whole temperature interval, phosphide phases M_3P and M_2P become stable below 450 °C, while the silicide G-phase becomes thermodynamically stable at temperatures below 250 °C. The predicted equilibrium volume fraction of the G-phase below 200 °C is large enough to become the subject of further investigations.

We note that the result of the present study on the stability of G-phase agrees with the result of thermodynamic analyses performed by Xiong et al. (2014) and Sprouster et al. (2016). In particular, the precipitate volume fraction (which for Mn-Ni-Si rich precipitates is similar to the volume fraction) has been reported by Wells et al. (2014) and Xiong et al. (2014) to be proportional to the sum of atomic concentrations of Ni, Mn, Si, and Cu and also to the atomic concentration of Ni. In the case considered in the present thermodynamic calculations, the maximum volume fraction of G-phase is limited by the amount of Mn and Ni in the alloy (since Si is in excess) and calculated to be slightly less than the sum of Ni and Mn atomic concentrations, in qualitative agreement with the findings by Wells et al. (2014) and Xiong et al. (2014). Importantly, the obtained temperature interval of the G-phase stability agrees with experimental observations by Miller et al. (2009) and Styman et al. (2015) who reported the LBP formation under low-temperature irradiation, identified the precipitates as the G-phase, and observed gradual dissolution of the precipitates during post-irradiation annealing at 450 °C.

5 Conclusions

Using *ab initio* calculations of point defect interactions and empirically based thermodynamic modelling, we show that precipitation of LBPs such as the G-phase (rich in Ni, Mn, and Si), M_2P and M_3P phosphides (M = Cr, Fe, Ni), and Mn-containing sulfide is thermodynamically possible, and that interactions of some solute elements with vacancies and self-interstitial atoms in iron matrix can promote precipitation of these phases kinetically. The total equilibrium volume of the predominant G-phase precipitates is found to be limited by the availability of Ni and Mn solutes in the alloy matrix and in the studied case is estimated to be about 0.5 %.

These conclusions are preliminary and qualitative. They are derived from *ab initio* calculations and simplified thermodynamic modelling, but are consistent with the previously published theoretical results and experimental observations. To derive more certain and quantitatively accurate conclusions about the expected volume fraction and number density of the precipitates (as well as about their effect on the mechanical properties of the insert material), further studies are necessary (including experimental efforts).

References

SKB's (Svensk Kärnbränslehantering AB) publications can be found at www.skb.com/publications.

Abrikosov I A, Niklasson A M N, Simak S I, Johansson B, Ruban A V, Skriver H L, 1996. Order-*N* Green's function technique for local environment effects in alloys. Physical Review Letters 76, 4203–4206.

Abrikosov I A, Simak S I, Johansson B, Ruban A V, Skriver H L, 1997. Locally self-consistent Green's function approach to the electronic structure problem. Physical Review B 56, 9319–9334.

Andersson J-O, Helander T, Höglund L, Shi P, Sundman B, 2002. Thermo-Calc & DICTRA, computational tools for materials science. Calphad 26, 273–312.

Bakker H, Bonzel H P, Bruff C M, Dayananda M A, Gust W, Horvath J, Kaur I, Kidson G V, LeClaire A D, Mehrer H, Murch G E, Neumann G, Stolica N, Stolwijk N A, 1990. Diffusion in solid metals and alloys. Berlin: Springer-Verlag.

Bonny D, Terentyev D, Bakaev A, Zhurkin E E, Hou M, Van Neck D, Malerba L, 2013. On the thermal stability of late blooming phases in reactor pressure vessel steels: an atomistic study. Journal of Nuclear Materials 442, 282–291.

Buschow K H J, Van Engen P G, Jongebreur R, 1983. Magneto-optical properties of metallic ferromagnetic materials. Journal of Magnetism and Magnetic Materials 38, 1–22.

Chiapetto M, Messina L, Becquart C S, Olsson P, Malerba L, 2017. Nanostructure evolution of neutron-irradiated reactor pressure vessel steels: Revised Object kinetic Monte Carlo model. Nuclear Instruments and Methods in Physics Research B 393, 105–109.

Domain C, 2006. *Ab initio* modelling of defect properties with substitutional and interstitial elements in steels and Zr alloys. Journal of Nuclear Materials 351, 1–19.

Domain C, Becquart C S, 2001. *Ab initio* calculations of defects in Fe and dilute Fe–Cu alloys. Physical Review B 65, 024103. doi:10.1103/PhysRevB.65.024103

Domain C, Becquart C S, 2005. Diffusion of phosphorus in α-Fe: an *ab initio* study. Physical Review B 71, 214109. doi:10.1103/PhysRevB.71.214109

Fikar J, Gröger R, Schäublin R, 2017. Effect of orientation of prismatic dislocation loops on interaction with free surfaces in BCC iron. Journal of Nuclear Materials 497, 161–165.

Frolov A A, Sidorenko F A, Krentsis R P, Gel'd P V, 1972. Peculiarities in the structure of $(Fe_xNi_{1-x})_2Si$ solid solutions. (Russian) Journal of Inorganic Chemistry (translated from Zhurnal Neorganicheskoi Khimii) 17, 1347–1348.

Furuseth S, Kjekshus A, 1965. On the properties of α-MnS and MnS_2. Acta Chemica Scandinavica 19, 1405–1410.

Gagné M (ed), 2004. The Sorelmetal book of ductile iron. Sorel-Tracy, Canada: Rio Tinto Iron & Titanium.

Gorbatov O I, Korzhavyi P A, Ruban A V, Johansson B, Gornostyrev Y N, 2011. Vacancy–solute interactions in ferromagnetic and paramagnetic bcc iron: *ab initio* calculations. Journal of Nuclear Materials 419, 248–255.

Gorbatov O I, Okatov S V, Gornostyrev Yu N, Korzhavyi P A, Ruban A V, 2013. Effect of magnetism on the solubility of 3d elements in bcc iron: Results of first-principle investigations. The Physics of Metals and Metallography 114, 642–653.

Gorbatov O I, Gornostyrev Yu N, Korzhavyi P A, Ruban A V, 2015. Effect of Ni and Mn on the formation of Cu precipitates in α-Fe. Scripta Materialia 102, 11–14.

Gorbatov O I, Delandar A H, Gornostyrev Yu N, Ruban A V, Korzhavyi P A, 2016. First-principles study of interactions between substitutional solutes in bcc iron. Journal of Nuclear Materials 475, 140–148.

Gurovich B, Kuleshova E, Shtrombakh Ya, Fedotova S, Maltsev D, Frolov A, Zabusov O, Erak D, Zhurko D, 2015. Evolution of structure and properties of VVER-1000 RPV steels under accelerated irradiation up to beyond design fluences. Journal of Nuclear Materials 456, 23–32.

Hornbogen E, 1961. Precipitation of phosphorus from alpha iron and its effect on plastic deformation. Transactions of the American Society for Metals 53, 569–589.

Khalaff K, Schubert K, 1974. Kristallstruktur von Fe_2Si(h). Journal of the Less-Common Metals 35, 341–345. (In German.)

Kolenda M, Szytuła A, Leciejewicz J, Maletka C, 1991. Magnetic properties of $Mn_6Ni_{16}Si_7$ and $Mn_3Cr_3Ni_{16}Si_7$. Journal of Magnetism and Magnetic Materials 96, 121–124.

Kolli R P, Seidman D N, 2008. The temporal evolution of the decomposition of a concentrated multicomponent Fe–Cu-based steel. Acta Materialia 56, 2073–2088.

Kudielka H, 1977. Die Kristallstruktur von Fe_2Si, ihre Verwandtschaft zu den Ordnungsstrukturen des α-(Fe, Si)-Mischkristalls und zur Fe_5Si_3-Struktur. Zeitschrift für Kristallographie, Kristallgeometrie, Kristallphysik, Kristallchemie 145, 177–189. (In German.)

Lindgren K, Boåsen M, Stiller K, Efsing P, Thuvander M, 2017. Evolution of precipitation in reactor pressure vessel steel welds under neutron irradiation. Journal of Nuclear Materials 488, 222–230.

Lukas H L, Fries S G, Sundman B, 2007. Computational thermodynamics: The Calphad method. Cambridge: Cambridge University Press.

Messina L, Nastar M, Garnier T, Domain C, Olsson P, 2014. Exact *ab initio* transport coefficients in bcc Fe–X (X = Cr, Cu, Mn, Ni, P, Si) dilute alloys. Physical Review B 90, 104203. doi:10.1103/PhysRevB.90.104203

Messina L, Nastar M, Sandberg N, Olsson P, 2016. Systematic electronic-structure investigation of substitutional impurity diffusion and flux coupling in bcc iron. Physical Review B 93, 184302. doi:10.1103/PhysRevB.93.184302

Miller M K, Russell K F, 2007. Embrittlement of RPV steels: an atom probe tomography perspective. Journal of Nuclear Materials 371, 145–160.

Miller M K, Chernobaeva A A, Shtrombakh Y I, Russell K F, Nanstad R K, Erak D Y, Zabusov O O, 2009. Evolution of the nanostructure of VVER-1000 RPV materials under neutron irradiation and post irradiation annealing. Journal of Nuclear Materials 385, 615–622.

Muhlholland M D, Seidman D N, 2011. Nanoscale co-precipitation and mechanical properties of a high-strength low-carbon steel. Acta Materialia 59, 1881–1897.

Ngayam-Happy R, Becquart C S, Domain C, 2013. First principle-based AKMC modelling of the formation and medium-term evolution of point defect and solute-rich clusters in a neutron irradiated complex Fe–CuMnNiSiP alloy representative of reactor pressure vessel steels. Journal of Nuclear Materials 440, 143–152.

Odette G R, Nanstad R K, 2009. Predictive reactor pressure vessel steel irradiation embrittlement models: issues and opportunities. JOM 61, 17–23.

Ohnuma T, Soneda N, Iwasawa M, 2009. First-principles calculations of vacancy–solute element interactions in body-centered cubic iron. Acta Materialia 57, 5947–5955.

Olsson P, Abrikosov I A, Vitos L, Wallenius J, 2003. *Ab initio* formation energies of Fe–Cr alloys. Journal of Nuclear Materials 321, 84–90.

Olsson P, Abrikosov I A, Wallenius J, 2006. Electronic origin of the anomalous stability of Fe-rich bcc Fe–Cr alloys. Physical Review B 73, 104416. doi:10.1103/PhysRevB.73.104416

Olsson P, Klaver T P C, Domain C, 2010. *Ab initio* study of solute transition-metal interactions with point defects in bcc Fe. Physical Review B 81, 054102. doi :10.1103/PhysRevB.81.054102

Perdew J P, Burke K, Ernzerhof M, 1996. Generalized gradient approximation made simple. Physical Review Letters 77, 3865. doi:10.1103/PhysRevLett.77.3865

Ruban A V, Korzhavyi P A, Johansson B, 2008. First-principles theory of magnetically driven anomalous ordering in bcc Fe–Cr alloys. Physical Review B 77, 094436. doi:10.1103/PhysRevB.77.094436

Rundqvist S, 1962. X-Ray investigations of the ternary system Fe–P–B. Some features of the systems Cr–P–B, Mn-P-B, Co–P–B and Ni–P–B. Acta Chemica Scandinavica 16, 1–19.

Saunders N, Miodownik A P, 1998. Calphad: calculation of phase diagrams: a comprehensive guide. New York: Pergamon.

Sencer B H, Kennedy J R, Cole J I, Maloy S A, Garner F A, 2009. Microstructural analysis of an HT9 fuel assembly duct irradiated in FFTF to 155 dpa at 443 °C. Journal of Nuclear Materials 393, 235–241.

SKB, 2010. Design, production and initial state of the canister. SKB TR-10-14, Svensk Kärnbränslehantering AB.

Soisson F, Fu C-C, 2007. Cu-precipitation kinetics in α-Fe from atomistic simulations: vacancy-trapping effects and Cu-cluster mobility. Physical Review B 76, 214102. doi:10.1103/PhysRevB.76.214102

Sprouster D J, Sinsheimer J, Dooryhee E, Ghose S K, Wells P, Stan T, Almirall N, Odette G R, Ecker L E, 2016. Structural characterization of nanoscale intermetallic precipitates in highly neutron irradiated reactor pressure vessel steels. Scripta Materialia 113, 18–22.

SSM, 2011. Granskning och utvärdering av SKB:s redovisning av Fud-program 2010. Rapport 2011:10, Strålsäkerhetsmyndigheten (Swedish Radiation Safety Authority).

Stiller K, Andrén H O, Andersson M, 2008. Precipitation in maraging and martensitic chromium steels – what can we learn using 3-DAP and EFTEM. Materials Science and Technology 24, 633–640.

Styman P D, Hyde J M, Parfitt D, Wilford K, Burke M G, English C A, Efsing P, 2015. Post-irradiation annealing of Ni–Mn–Si-enriched clusters in a neutron-irradiated RPV steel weld using Atom Probe Tomography. Journal of Nuclear Materials 459, 127–134.

Was G S, Jiao Z, Getto E, Sun K, Monterrosa A M, Maloy S A, Anderoglu O, Sencer B H, Hackett M, 2014. Emulation of reactor irradiation damage using ion beams. Scripta Materialia 88, 33–36.

Wells P B, Yamamoto T, Miller B, Milot T, Cole J, Wu Y, Odette G R, 2014. Evolution of manganese-nickel-silicon-dominated phases in highly irradiated reactor pressure vessel steels. Acta Materialia 80, 205–219.

Xiong W, Ke H, Krishnamurthy R, Wells P, Odette G R, Morgan D, 2014. Thermodynamic models of low-temperature Mn–Ni–Si precipitation in reactor pressure vessel steels. MRS Communications 4, 101–105.

Arkitektkopia AB, Bromma, 2018

SKB is responsible for managing spent nuclear fuel and radioactive waste produced by the Swedish nuclear power plants such that man and the environment are protected in the near and distant future.

skb.se